AJNR

NMR Demonstration of Cerebral Abnormalities: Comparison with CT

Michael Brant-Zawadzki, Peter L. Davis, Lawrence E. Crooks, Catherine M. Mills, David Norman, Thomas H. Newton, Phil Sheldon and Leon Kaufman

AJNR Am J Neuroradiol 1983, 4 (2) 117-124
http://www.ajnr.org/content/4/2/117

NMR Demonstration of Cerebral Abnormalities:
Comparison with CT

Michael Brant-Zawadzki[1, 2]
Peter L. Davis[1, 3]
Lawrence E. Crooks[1, 3]
Catherine M. Mills[1, 3]
David Norman[1]
Thomas H. Newton[1]
Phil Sheldon[1, 3]
Leon Kaufman[1, 3]

Sixty-eight patients with a wide spectrum of brain pathology were imaged with both computed tomography (CT) using a G.E. 8800 scanner and nuclear magnetic resonance (NMR) imaging with a 3.5 kG prototype device. NMR was more advantageous in the detection and/or characterization of pathology in 20 of the 68 patients, especially when demyelination was part of the disease process or when the lesion was obscured on CT by beam-hardening artifact. Punctate foci of calcification identified on CT were not detected on NMR, but larger calcifications were seen. NMR was sensitive to detection of both normal and abnormal vascular structures. The ability of NMR to differentiate among different pathologic entities remains to be fully evaluated. NMR currently complements CT in the evaluation of many disease entities and may actually supplant CT in some. The full future potential of NMR and its role with respect to CT has only begun to be elucidated.

The rapid development of nuclear magnetic resonance (NMR) imaging is documented by many recent reports, several of which include representative clinical material [1–8]. Clinical studies have begun to clarify the future role of NMR. However, current NMR equipment is far from standardized. Both hardware and imaging technique differ substantially among the imagers now being used. Certain techniques are already proving more useful than others in delineating pathology [7–9]. Because of the rapidly changing technology, clinical efficacy questions regarding NMR are still somewhat premature. Comparison studies with CT must be evaluated with the understanding that one is comparing the technologies at very different stages of maturity.

The impressive quality of the few images already published has fueled increasing interest in the diagnostic impact of NMR. The intent of this communication is to summarize initial experience at the University of California, San Francisco, in NMR imaging of patients with a broad spectrum of cerebral disease and to compare the results with CT. Ultimately the utility of NMR and its role with respect to CT must await determination of the optimal imaging techniques within each disease category, but sufficient results have already been obtained to illustrate the clinical usefulness of NMR in selected cases even in its current state of development and to indicate fertile areas of further investigation in order to better assess its future potential.

Subjects and Methods

A total of 75 subjects underwent cerebral NMR studies over a 6-month period. Seven were normal volunteers. The 68 patients studied were mostly ambulatory and ranged in age from 2 months to 80 years. Sixty of the 68 patients had a firm diagnosis based on clinical and/or pathologic biopsy criteria.

Twenty-nine patients suffered from degenerative disorders (multiple sclerosis, Parkinson disease, Huntington chorea, Wilson disease, cerebellar degeneration, Meige syndrome, and Jakob-Creutzfeldt disease). Twelve patients had primary intracranial tumors including

This article appears in the March/April 1983 issue of *AJNR* and the May 1983 issue of *AJR*.

Received September 17, 1982; accepted after revision November 12, 1982.

Presented at the XII Symposium Neuroradiologicum, Washington, DC, October 1982.

This work was supported in part by Diasonics (NMR), Inc., and by U.S. Public Health Service grant CA 32850 (National Cancer Institute).

[1] Department of Radiology, University of California, San Francisco, CA 98143.

[2] Department of Radiology, San Francisco General Hospital, Room 1X55D, 1001 Potrero Ave., San Francisco, CA 94110. Address reprint requests to M. Brant-Zawadzki.

[3] Radiologic Imaging Laboratory, University of California, San Francisco, South San Francisco, CA 94080.

***AJNR* 4:117–124, March/April 1983**
0195–6108/83/0402–0117 $00.00

glioma, meningioma, germinoma, pituitary adenoma, medulloblastoma, cerebellar hemangioendothelioma, teratoma, and epidermoid. Two patients were evaluated for metastases, one with known lesions, the second for screening purposes. Six patients had neurologic sequelae of infection (postinfectious encephalitis in five, brain abscess in one). Five patients had ischemic lesions, four had arteriovenous malformations (AVMs), two had suffered trauma, and eight were evaluated for neurologic abnormalities of uncertain etiology.

In 66 patients, a CT scan obtained within 1 day to 4 weeks of the NMR study was available for comparison. Most were scans obtained on a third generation CT scanner (G.E. 8800) at our institution.

The NMR studies were performed using an imager based on a 3.5 kG superconducting magnet, with a useful aperture of 55 cm, which is the aperture of the body coil. The head coil has an aperture of 25 cm and a saddle shape. Radiofrequency (RF) power levels do not exceed 7 W average power into the coil. Magnetic field gradients do not exceed 1 G/cm, and have a rise time of 1 msec. The magnet and patient bed are within a copper-mesh enclosure, which provides shielding against external RF sources. The matrix size of the resulting images is 128 × 128. Each pixel measures 1.7 mm (X,Y). Slice thickness is 7 mm. Both spin-echo (SE) and inversion-recovery (IR) techniques were used in most patients. The former retain both T_1 and T_2 information in the images and offer higher signal-to-noise (S/N) ratio, whereas the latter are strongly T_1-dependent and can optimize gray-white matter differences.

Our imaging techniques, their variations, and consequent impact on the information content and quality of resulting images are fully discussed in two recent reports [6, 9]. Summarized briefly, protons (hydrogen nuclei) spin and act as magnetic dipoles. When placed in a strong magnetic field, they tend to become aligned with it, producing a net magnetic vector in the sample. An RF pulse of a specific frequency (dependent on the strength of the magnetic field) is used to alter the energy state of the protons and displaces the net magnetic vector by an amount determined by the strength and duration of the pulse. After the pulse is removed, the protons emit energy in the form of an RF signal as they return to their original orientation. When a gradient is introduced in the magnetic field, the frequency emitted by the irradiated protons will vary with their positions in the gradient.

When protons are placed in a magnetic field, their alignment (or realignment after an RF disturbance) occurs exponentially, with a time constant T_1. T_1 is the "spin-lattice" relaxation time and reflects the interaction of the hydrogen nucleus with its molecular environment. In forming an image the RF pulses must be applied repetitively. After each pulse the net proton alignment or magnetization of the sample is zero. Rapid repetition would not allow much magnetization to be reestablished, and little signal would be seen. Thus, a certain time interval b is introduced between successive RF pulses. As the interval b increases, the magnetization and signal increase, but so does the imaging time. These considerations, and the fact that the choice of b affects the contrast between tissues with different T_1 values, are taken into account in selecting b.

The RF pulse not only alters the magnetization of the sample, but induces resonance of the individual protons in such a way that they resonate in a coherent manner. The signal emitted by the protons decays as local inhomogeneities of magnetic field cause the resonance of protons within the sample to lose coherence. The amount of signal available then decays exponentially in time, with a time constant characterized by the T_2, or "spin-spin" relaxation time, which reflects magnetic interactions between protons. The interval between application of an RF pulse and reception of a signal (an SE) is chosen by the instrument parameter a. As a is increased, signal decreases, and contrast between tissues with different values of T_2 changes.

Appropriate variation of the instrument parameters a and b in the SE technique is important since it optimizes the ability to obtain contrast on the basis of T_1 and T_2 tissue characteristics. Also, the ability to appreciate flow within blood vessels is affected by the choice of instrument parameters. Rapidly moving protons traverse the imaged plane and produce relatively little signal. Signal intensity from slowly moving protons, however, can be quite high, and for any given velocity varies depending on the choice of a and b parameters [9, 10].

Effects of Relaxation Time on Gray Scale

Although the parameters T_1, T_2, and flow represent intrinsic tissue properties, the translation of these parameters onto the NMR image is dependent on the particulars of the imaging technique used to form that image.

Let us first consider the effect of repeating the imaging sequence at intervals b. If we assume that a single exponential characterizes tissue T_1, the amount of intensity I in the image becomes

$$I = H\, f(v)[1 - exp\ (-b/T_1)], \quad (1)$$

where H is the hydrogen density and f(v) is a function of the proton velocity.

If the signal is obtained immediately after excitation, it will not have undergone any T_2 decay. This signal is called a free induction decay (FID) and yields intensities as shown by equation 1. If, instead, pulses are manipulated so as to produce an SE signal,

$$I = H\, f(v)\, exp(-a/T_2)\, [1 - exp\ (-b/T_1)]. \quad (2)$$

Note that f(v) is not the same function in equations 1 and 2. Aside from different response to flow, the FID and SE signals differ in that the former has the strongest signal, but no T_2 dependence. While strong signals undoubtedly yield better instrumental S/N levels, the significant component of the signal in the image generated is given by the difference between two tissues that one is trying to distinguish. To the extent that differences due to T_2 contribute to tissue characterization, FID signal acquisition omits information when compared with SE. For this reason, we do not use the FID imaging technique.

Considering the tissue constants T_1 and T_2 in equation 2, we can see that I will increase, or show brightness, when T_1 is shortened or T_2 is lengthened. Also, this equation shows that when T_1 is very long compared with b, intensity is low independently of the value of T_2. Conversely, when T_2 is short compared with a, intensity is also low even if T_1 is short. Note that these interrelationships of tissue and instrument parameters can cause a fortuitous cancellation of intensity differences on any single image. Therefore, calculations of T_1 and T_2 are sometimes necessary and can be obtained from SE images performed with two variables of a and b each, since I is given by the instrument. Such calculations also permit synthesis of calculated images that display T_1 and T_2 values of tissue in a gray scale, which, by convention, shows long T_1 and T_2 as bright, short T_1 and T_2 as dark. Such depiction of altered T_1 or T_2 relaxation time in a lesion relative to a "control" area in the brain is useful for comparing results from different institutions, since absolute numerical T_1 and T_2 tissue values depend on the instrument and vary with the method used to obtain them.

Another technique has been used to introduce T_1 dependence in the NMR image. The magnetization vector is first reversed and allowed to recover for a time Tr, the sequence repeated at intervals b. If Tr is carefully chosen, tissues with long T_1 values can be observed at times where their signal is nearly zero, while shorter T_1 values are still yielding considerable signal. This technique is the

IR. IR has been used because it produces exquisite differentiation between gray and white matter. However, IR images take longer to obtain, have lower S/N levels, and, in our experience, have less sensitivity to contrast differences between normal and abnormal tissue. It is worth noting that for IR technique where $b \gg Tr$, the response of the system becomes similar to that of an FID or SE technique with a long value of b [8].

Results

Of 70 patients, 67 had successful NMR studies, two patients declined to complete the study due to claustrophobia, and in our first case the level of the lesion was inadvertently missed. In no other cases did NMR miss a lesion that was present on the comparable CT scan. In 16 patients, NMR either detected an abnormality missed with CT or showed more lesions than did CT in cases with multifocal disease. In another four patients, either the nature or extent of the abnormal process was more fully characterized with NMR compared with CT. Although detection of abnormality with NMR seemed more sensitive than with CT, absolute differentiation between certain pathologic entities still proved problematical. These overall results are best analyzed within the major categories of disease studied.

Degenerative Disease

The superior sensitivity of NMR in comparison with CT was most impressive in 13 patients with multiple sclerosis. In 12 of these, multiple lesions not seen with CT were detected in the periventricular white matter with both SE and IR techniques. CT showed no focal lesions in six of these cases and showed fewer focal lesions than did NMR in six others. The last patient's NMR study was technically flawed but suggested a lesion. This patient refused a CT study at the time of NMR imaging, having had a normal study 5 years before.

The lesions appeared as high-intensity foci on the SE image techniques designed to emphasize prolonged T_2 relaxation times. The IR images detected fewer lesions than did the pulse-echo images, mostly due to problems with lesion-to-background contrast differentiation in regions close to the gray-white matter interface, since the foci of demyelination are of similar low intensity to the gray matter on these images. The SE images did not have this limitation because the intensity of the lesion was obviously greater than the background (fig. 1). Of interest, the SE technique depicted the lesions as appearing larger and more coalescent than did the IR technique. Lesions in regions poorly studied with CT due to beam-hardening artifacts (posterior fossa, brainstem) were easily detected with NMR.

Abnormalities of the basal ganglia or cortex in patients with degenerative diseases that predominantly affect the gray matter (Huntington chorea and Jakob-Creutzfeldt disease) were seen as regional atrophy in NMR and CT studies. One patient with long-standing Wilson disease exhibited generalized atrophy on both studies, while the second patient with Wilson disease evidenced more specific degenerative changes within the lenticular nucleus on NMR than on CT, although punctate foci of calcification seen with the latter method could not be identified on NMR (fig. 2). The patients with Parkinson disease showed no abnormality with either method, nor did the patient with Meige orofacial dystonia. Cerebellar atrophy was equally well seen with CT and NMR.

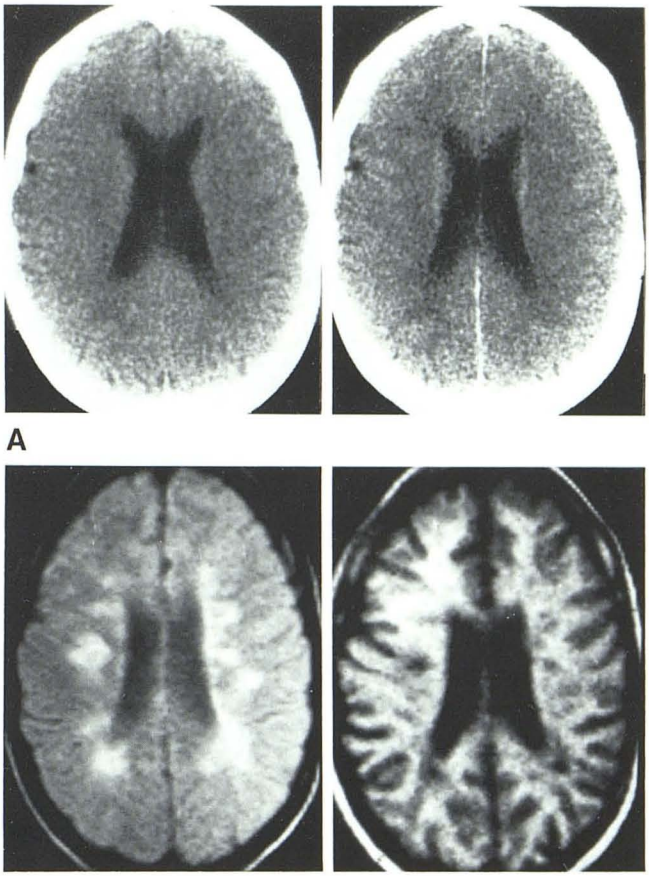

Fig. 1.—Multiple sclerosis. **A**, Pre- (left) and post- (right) contrast CT scans at level of lateral ventricles show no abnormality. **B**, SE (left) and IR (right) NMR images at same level reveal multiple focal lesions in periventricular white matter. Note superior contrast difference between lesions and normal brain with SE technique.

Tumors

Of the 14 patients studied for tumors with both NMR and CT, 11 showed the lesion on both NMR and CT, two on NMR only, while one patient evaluated for metastases had no lesion seen with either study. A cerebellar hemangioendothelioma was missed on CT due to beam-hardening artifact in the posterior fossa, but was visualized (and subsequently proven at autopsy) on NMR images. The second

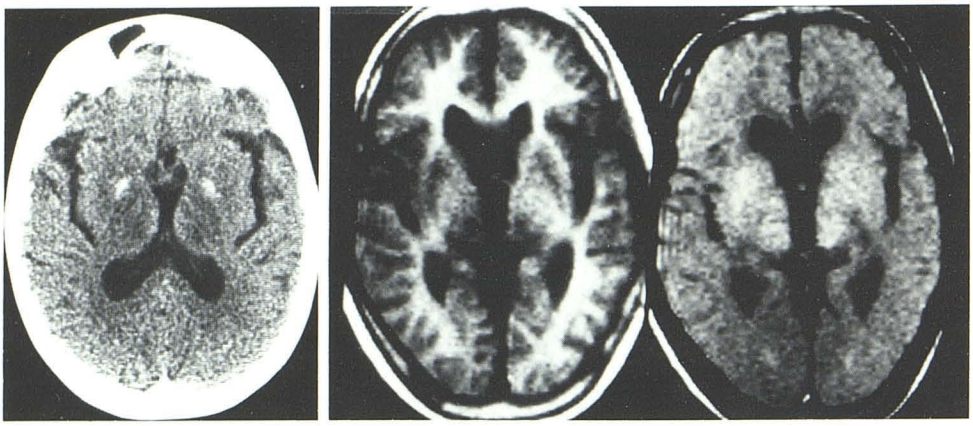

Fig. 2.—Wilson disease. **A**, CT shows generalized hypodensity in basal ganglia with punctate calcification. **B**, NMR images at comparable level in basal ganglia (slight difference in patient positioning compared with **A**) fail to depict punctate calcification. However, IR image (left) reveals characteristic degenerative change in lenticular nuclei, seen as low-intensity crescents, and similar abnormal intensity in thalami. SE image (right) shows abnormalities as high-intensity regions.

false-negative CT study occurred in a patient with multifocal metastases treated with radiation and steroids, in whom NMR depicted high-intensity foci at three sites (one of which was biopsied). In addition, two patients with abnormal CT studies had lesions that were better characterized with NMR. In one patient, an erosive lesion of the left petrous apex seen on CT showed intensity characteristics like those of subcutaneous fat on the variable SE NMR sequences; indeed, a teratoma with a lipomatous component was found at surgery (fig. 3). In the second patient, a prominent contrast-enhanced structure was seen in back of the third ventricle but was difficult to differentiate from large internal cerebral veins. NMR verified a soft-tissue neoplasm; a germinoma was found at surgery.

All the tumors except the epidermoid and medulloblastoma were seen as high-intensity areas on SE images, with the meningioma and brainstem glioma also having low-intensity foci (presumably calcium). The low intensity of the epidermoid and medulloblastoma was related to their long T_1 relaxation time. It is of interest that the medulloblastoma was isodense on CT before intravenous contrast injection. This patient also had an associated obstructive hydrocephalus with interstitial edema; both processes were well delineated with NMR and CT.

The other high-intensity lesions had no differentiating feature on either NMR or CT other than location. Determining what part of the lesion was tumor as opposed to surrounding edema was problematical on NMR. NMR did show high-intensity regions in the adjacent cerebellum of a young patient with a long-standing brainstem glioma. Whether this represented subclinical tumor spread or was related to radiation therapy remains unknown (fig. 4). One of the patients with a pituitary adenoma had a severe allergy to contrast agents, thus the NMR study offered more information than the noncontrast CT. In one other patient with a pituitary tumor seen on CT and studied early in our NMR experience, sections at the level of the sella were inadvertently not obtained.

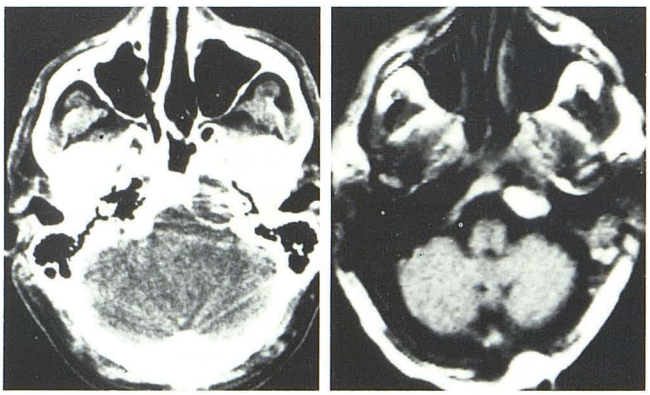

Fig. 3.—Teratoma of petrous apex. **A**, CT shows destructive lesion in left petrous apex. **B**, SE image using variable parameters revealed high-intensity lesion at this site, with T_1 and T_2 values consistent with fat. Biopsy showed teratoma with lipomatous component.

Postinfectious Lesions

Four of five patients studied in this group had sequelae of infection including foci of demyelination and encephalomalacia, the fifth showing no abnormality on either study. The former lesions were equally well seen with NMR (as small areas of high intensity similar to those seen in multiple sclerosis) and CT, except for one case that exhibited signs referable to the brainstem where NMR showed abnormality and CT did not, and another case where NMR showed a second lesion not seen with CT (fig. 5). The sixth patient had a resolving brain abscess that was equally well evaluated with NMR and contrast-enhanced CT. The IR technique showed the abscess as a low-intensity cavity surrounded by normal brain. SE technique designed to emphasize prolonged T_2 showed localized high intensity suggesting edema adjacent to the lesion.

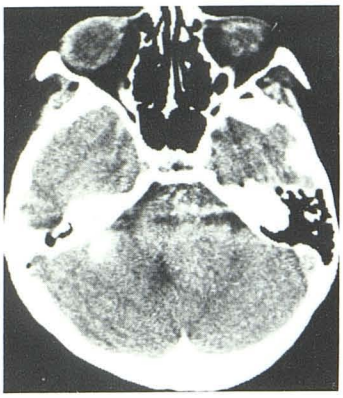

Fig. 4.—Brainstem glioma (status postradiation). **A**, CT after intravenous contrast administration depicts asymmetric enlargement of pons, displacement of fourth ventricle, and enhancing focus in right cerebellopontine angle. Note interpetrous beam hardening artifact. **B**, Axial NMR images show lesion in brainstem and cerebellum with greater contrast. Relatively higher intensity of left cerebellum compared with right and relative high intensity of lesion in right cerebellopontine angle. This is especially true on 56 msec sampling (right), which also shows extension of tumor into hypothalamus (*arrow*), when compared with 28 msec image (left). **C**, Two adjacent midsagittal sections depict pontine glioma and extent into hypothalamus (*arrow*).

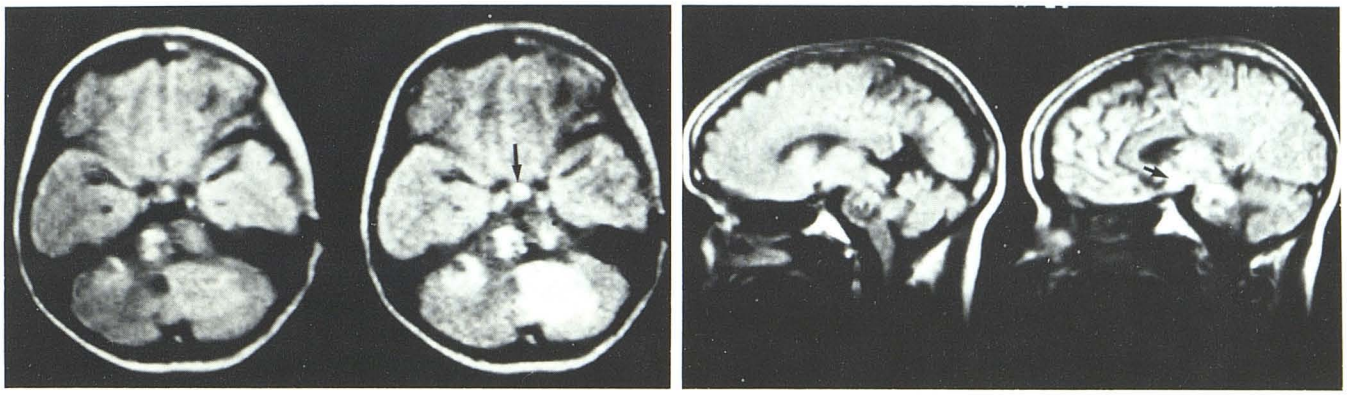

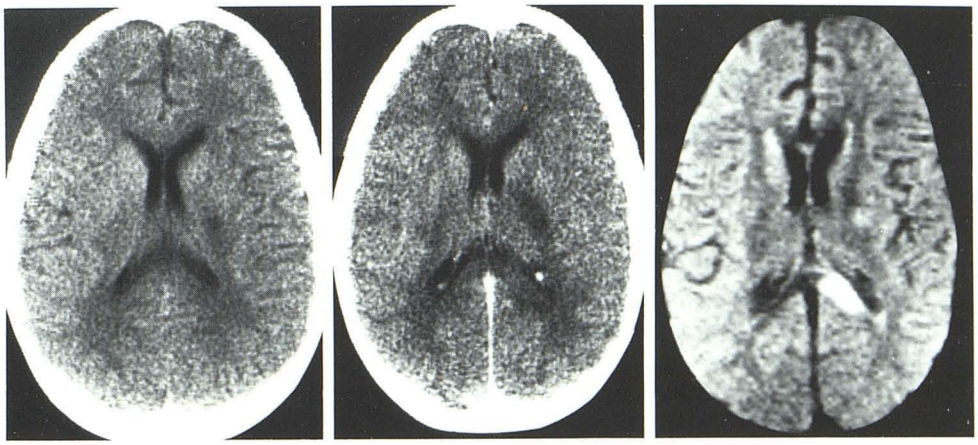

Fig. 5.—Postinfectious encephalitis. CT before (**A**) and after (**B**) intravenous contrast shows nonenhancing low-density lesion in left internal capsule. **C**, SE NMR image at comparable level depicts high-intensity focus not only in left internal capsule but also one in left major (posterior) forcep of corpus callosum.

A **B** **C**

Infarcts

Focal brain infarction was seen in four of five patients with both NMR and CT, and NMR study showing the extent of involvement to better advantage both in acute and subacute lesions (figs. 6–8). The fifth patient with a known chronic occlusion of the left carotid artery showed absence of his left internal carotid artery at the cavernous sinus level on NMR, and ipsilateral atrophy was noted on both NMR and CT.

One patient had a hemorrhagic infarct. The appearance of the lesion differed from the other infarcts seen with NMR in that its intensity was greater (fig. 8). Unlike the other infarctions, the hemorrhagic infarct also showed high inten-

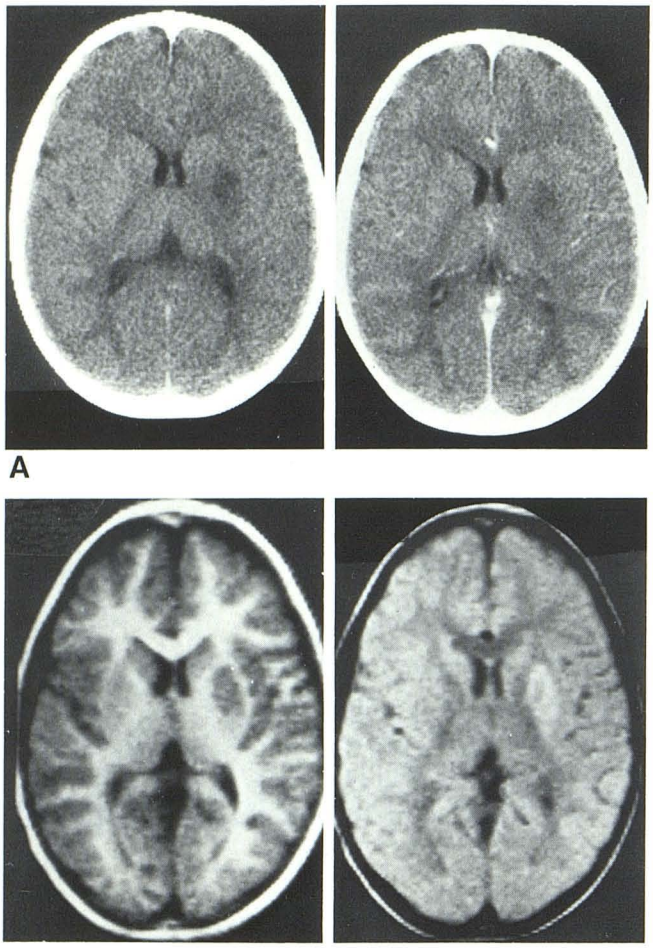

Fig. 6.—Acute basal ganglia infarct. **A**, CT at level of frontal horns shows hypodense lesion in left globus pallidus (left), which does not enhance after intravenous contrast administration (right). **B**, NMR images 4 days after stroke depict lesion as low-intensity focus on IR image due to its lengthened T_1 (left), whereas it shows as a high-intensity focus on second echo SE image due to its long T_2.

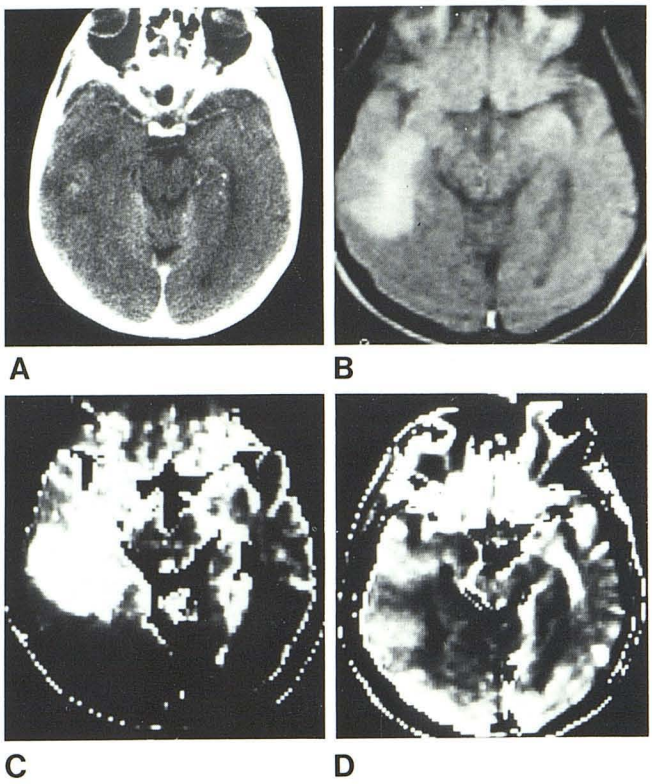

Fig. 7.—Subacute infarct. **A**, CT 4 days after right hemispheric infarction reveals inhomogenous lesion with slight contrast enhancement in right temporal lobe. **B**, SE NMR image shows area of high intensity 17 days after insult. Calculated images indicated prolongation of T_2 relaxation (bright area, **C**) is responsible for this intensity; T_1 in lesion was similar to normal brain (**D**).

sity on the image obtained with a pulse sequence that stressed short T_1 characteristics, suggesting a hemorrhagic component. Indeed, T_1 and T_2 calculations verified a short T_1 relaxation time in the hemorrhagic component and prolongation of T_2 relaxation in the periphery, correlating with edema. Two months after the insult, CT showed subtle focal low attenuation at the site of the hemorrhage, whereas NMR depicted an obvious residual lesion consistent with clot.

AVMs

Because protons that rapidly traverse the imaged volume return relatively little signal, vessels are identifiable on NMR images as tubular structures of low intensity. Abnormalities of flow may increase this low intensity appearance depending on the pulse sequence used [9, 10]. High-flow AVMs have a characteristic appearance on NMR images, much like on CT, and were easily diagnosed in three patients (fig. 9). A fourth patient harbored two "cryptic" AVMs that showed an atypical CT appearance suggesting neoplasms. Their NMR appearance was more specific with very high-intensity centers due to short T_1 relaxation consistent with thrombus surrounded by more inhomogeneous periphery (fig. 10).

Trauma

One of our two patients with trauma refused the study due to claustrophobia. The second patient's extraaxial fluid collections and postsurgical abnormalities of brain parenchyma were better delineated with NMR than with CT, as previously reported [9]. However, bone defects were more difficult to delineate.

Unknown

This group consisted of eight patients. Two patients had seizures. Unexplained progressive aphasia, spasmotic torticollis, supranuclear palsy, pseudotumor cerebri, and an unclassified degenerative disorder were the other entities studied. Three patients showed lesions; in all three the abnormality was seen on NMR and CT. One of the seizure patients had a CT and NMR defect that looked much like a

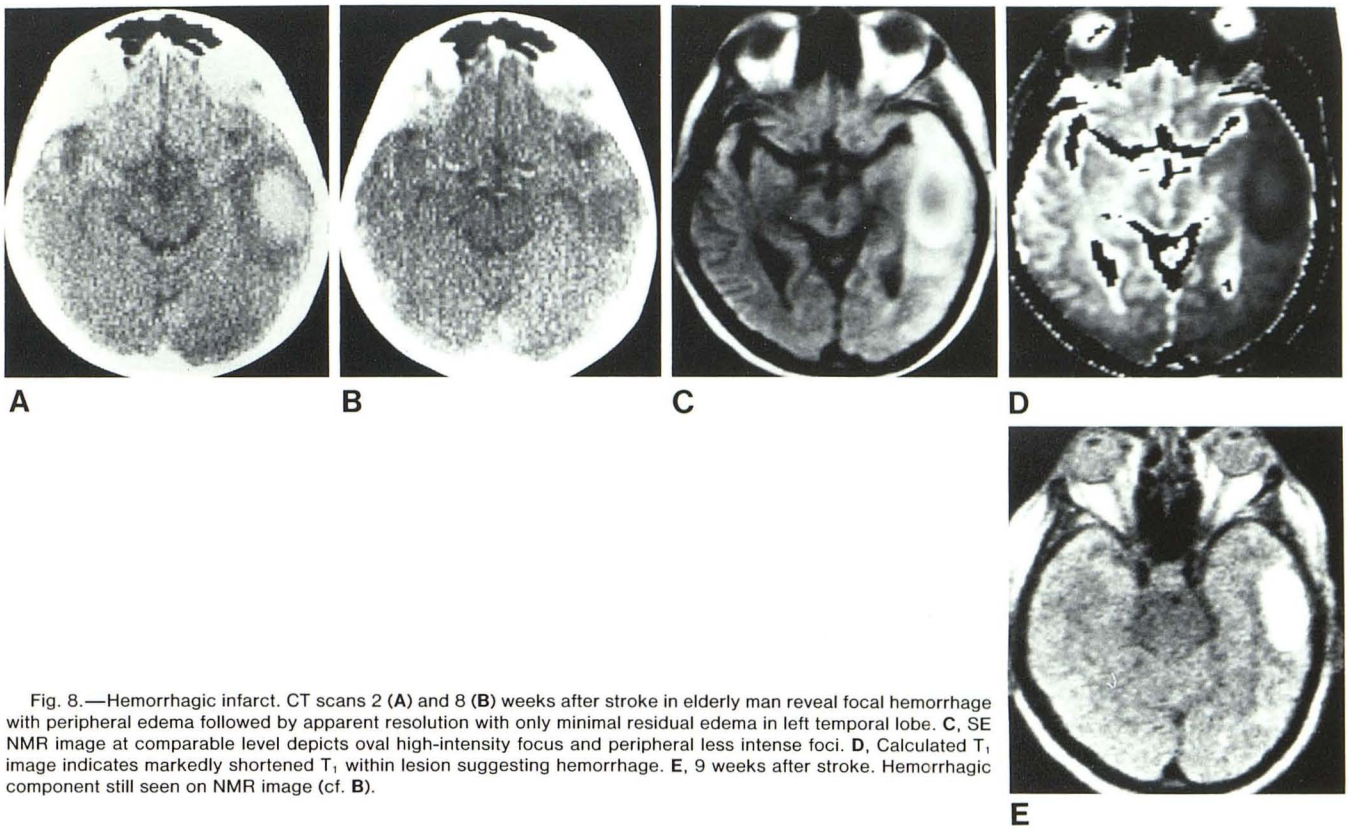

Fig. 8.—Hemorrhagic infarct. CT scans 2 (**A**) and 8 (**B**) weeks after stroke in elderly man reveal focal hemorrhage with peripheral edema followed by apparent resolution with only minimal residual edema in left temporal lobe. **C**, SE NMR image at comparable level depicts oval high-intensity focus and peripheral less intense foci. **D**, Calculated T_1 image indicates markedly shortened T_1 within lesion suggesting hemorrhage. **E**, 9 weeks after stroke. Hemorrhagic component still seen on NMR image (cf. **B**).

Fig. 9.—AVM. Axial NMR image shows characteristic serpiginous vessels with little signal within due to fast flow.

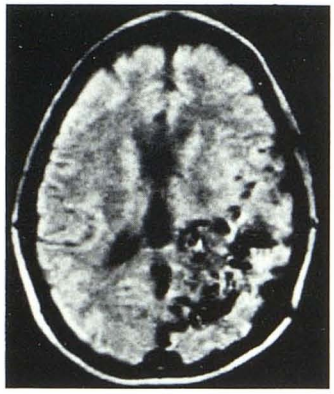

cryptic AVM, and her long history and young age (8 years) supported that diagnosis. The second lesion was symmetric degenerative calcification of both basal ganglia regions seen on CT and NMR (as areas of no signal) in a 25-year-old seizure patient with an unclassified degenerative brain disorder. One patient with clinically classic pseudotumor cerebri was found to have a focal mass in the right occipital region on both modalities. Extensive low attenuation of the white matter on CT and high intensity in the white matter on NMR (due to prolongation of T_2) suggested marked cerebral edema in both hemispheres. No histologic diagnosis was available at the time of this report.

Discussion

Our initial experience indicates that cerebral NMR imaging has considerable diagnostic potential, with several advantages over CT already apparent, but certain limitations exist at the present stage of development.

The depiction of brain anatomy and its major components (i.e., the gray and white matter) is superior to that offered by CT, especially in regions where beam-hardening artifact occurs on CT images. NMR is more sensitive to the presence of brain abnormalities than is CT by virtue of its superior contrast resolution, and does not require the use of ionizing radiation nor the injection of iodinated contrast material. This sensitivity is especially evident in foci of demyelination and/or edema of the white matter.

The ability of CT to discriminate between different disease entities is nonspecific in most cases, but accumulated experience over the years in visualization of certain abnormalities, coupled with their anatomic distribution, appearance after intravenous contrast administration, and clinical presentation, often permits a concise differentiatial diagnosis. Experience in differentiation of various pathologic entities with NMR is accumulating. Hemorrhage and brain edema have a similar high-intensity appearance on SE images, the former due to short T_1 relaxation time [4], the latter due to the prolonged T_2 relaxation time [9]. Therefore, these entities are easily differentiated with calculation of T_1 and T_2 relaxation times. Some tumors appear as low-inten-

Fig. 10.—Angiographically cryptic AVM. **A**, Contrast-enhanced sections from CT study in young patient reveal two lesions simulating neoplasms. High density prior to contrast. Cerebral angiogram showed nonspecific mass effect. **B**, Axial SE NMR image shows both lesions, with high-intensity center (shortened T_1 was calculated within) surrounded by less intense foci (lengthened T_2 was present), suggesting clot with peripheral edema. Thrombosed AVM was found at surgery. **C**, Sagittal section through center of right hemispheric lesion depicts similar characteristics as those of thrombus in fig. 8C.

sity foci, but most show high-intensity regions. Differentiating benign from malignant lesions, or separation of such lesion from adjacent edema may be difficult; further experience with T1 and T_2 calculations and different imaging sequences is needed before a definitive statement can be made. Punctate calcification can be missed with NMR but larger foci are easily detected as low-intensity regions. Vessels with normal flow are easily seen; abnormal or absent flow may prove identifiable.

The NMR appearances ascribed to different lesions in this report (and others) must be interpreted in the context of the type of magnet and imaging sequences employed and the variables introduced during those sequences. Until more standardization of NMR technology occurs, comparison with results from the other institutions is difficult. Since any one particular imaging technique may miss pathology because the specific excitation sequence used causes a fortuitous cancellation of diagnostic signal information from a given lesion [7, 9], care must currently be taken to obtain information with a variety of techniques in any one patient.

Our series is by no means a rigorous comparative study of NMR versus CT. The lesions in most cases were known to be present on CT before the NMR study, and no double blind reading protocol was used. Since our NMR techniques were and are being continually refined, this report is meant only to define the capabilities of NMR at a given point in its development and to suggest those areas in which it might complement a CT study. Whether it can totally supplant CT in some of these disease entities remains to be fully determined.

Certainly the potential of NMR is enticing. More sensitive detection of pathology including demyelination and brain edema should facilitate earlier intervention and more specific monitoring of therapy in afflicted patients. The inherent potential for broader characterization of soft-tissue differences without use of ionizing radiation is certainly a benefit, and might well be aided by use of paramagnetic contrast agents [11]. Also, the possible quantification of flow within normal and abnormal vessels deserves intense study. In view of the possibilities it is difficult to restrain the current enthusiasm and pressure for commercialization of the technology, but some restraint is important in the objective and orderly actualization of this technology's full potential.

REFERENCES

1. Holland GN, Hawkes RC, Moore WS. Nuclear magnetic resonance (NMR) tomography of the brain: coronal and sagittal sections. *J Comput Assist Tomogr* **1980**;4:429–433
2. Young IR, Burl M, Clarke GJ, et al. Magnetic resonance properties of hydrogen: imaging the posterior fossa. *AJR* **1981**;137:895–901.
3. James AE Jr, Partain CL, Holland GN, et al. Nuclear magnetic resonance imaging: the current state. *AJR* **1982**;138:201–210
4. Young IR, Bailes DR, Burl M, et al. Initial clinical evaluation of a whole body nuclear magnetic resonance (NMR) tomography. *J Comput Assist Tomogr* **1982**;6:1–18
5. Alfidi RJ, Haga JR, Yousef SJ, et al. Preliminary experimental results in humans and animals with a superconducting, whole-body, nuclear magnetic resonance scanner. *Radiology* **1982**;143:175–181
6. Crooks L, Arakawa M, Hoenninger J, et al. Nuclear magnetic resonance whole-body imager operating at 3.5 KGauss. *Radiology* **1982**;143:169–174
7. Buonanno FS, Pykett IL, Brady TJ, et al. Clinical relevance of two different nuclear magnetic resonance (NMR) approaches to imaging of a low grade astrocytoma. *J Comput Assist Tomogr* **1982**;6:529–535
8. Bydder GM, Steiner RE, Young IR, et al. Clinical NMR imaging of the brain: 140 cases. *AJNR* **1982**;3:459–480, *AJR* **1982**;139:215–236
9. Crooks LE, Mills CM, Davis PL, et al. Visualization of cerebral and vascular abnormalities by NMR imaging: the effects of imaging parameters on contrast. *Radiology* **1982**;144:843–852
10. Crooks L, Sheldon P, Kaufman L, Rowan W, Miller T. Quantification of obstructions in vessels by nuclear magnetic resonance. *IEEE Trans Nucl Sci* **1982**;29:1181–1185
11. Brady TJ, Goldman MR, Pykett IL, et al. Proton nuclear magnetic resonance imaging of regionally ischemic canine hearts: effect of paramagnetic proton signal enhancement. *Radiology* **1982**;144:343–347